RSC Advances

ROYAL SOCIETY OF CHEMISTRY

www.rsc.org/advances

Journal Name

ARTICLE TYPE

Cite this: DOI: 10.1039/xxxxxxxxxx

First principles study of ruthenium(II) sensitizer adsorption on anatase TiO_2 (001) surface

Hao Yang,[ab] Jia Li,[†a] Gang Zhou,[c] Sum Wai Chiang,[a] Hongda Du,[a] Lin Gan,[a] Chengjun Xu,[a] Feiyu Kang,[a] and Wenhui Duan[de]

Received Date
Accepted Date

DOI: 10.1039/xxxxxxxxxx

www.rsc.org/journalname

We present a systematic investigation on the adsorption behavior of the highly efficient ruthenium (II) sensitizer (N3) on anatase TiO_2 (001) surface based on density functional theory. Three preferable configurations can be formed by exploiting two or three carboxylic groups attach to the TiO_2 surface, with their adsorption energies differing slightly. Whereas, the interplay of N3 with (001) surface is considerably stronger than that of N3 with (101) surface, resulting in a larger dye coverage on the (001) surface. The energy gap of N3 sensitizer, determining the absorption spectrum, decreases about 0.12 eV upon adsorption, suggesting an ever larger range of absorption spectrum than isolated N3 molecule. Moreover, the higher conduction band minimum of TiO_2 (001) surface with N3 adsorption, compared with that of (101) surface, indicates the higher open circuit potential. These results provide a clue to understand the high solar light-to-electricity conversion efficiency of dye sensitized solar cells with TiO_2 nanocrystals exposing high percentage of {001} faces.

1 Introduction

Dye sensitized solar cells (DSSCs) have attracted enormous interests over the past decades for their low cost and high efficiency in converting solar energy to electricity.[1,2] In contrast to the conventional *p-n* junction photovoltaic device where the semiconductor assumes both the task of light absorption and charge carrier transport,[3] a DSSC uses a dye sensitizer to absorb the solar radiation and transfer the photo-excited electrons to its wide band gap semiconductor electrode. In this way, the absorption light wavelength is extended to the visible region, which constitutes most of the solar radiation. The overall conversion efficiency (η) of the DSSC is defined as: $\eta = (i_{ph})(V_{oc})(\mathrm{ff})/I_s$, where i_{ph} is photocurrent density at short circuit, V_{oc} is the open circuit voltage of the cell (the difference between the quasi-Fermi level of the semiconductor under illumination and the redox potential of the mediator), ff is the fill factor and I_s is the intensity of the incident light. Therefore, to improve the efficiency, the product of V_{oc} and i_{ph} should be optimized. In a photovolatic device, photoanode is perhaps one of the most important components, which directly determines the photocurrent (i_{ph}), open-circuit photovoltage (V_{oc}) and cycling performance of the cell. In general, photoanode materials now are mainly composed of metal oxide semiconductor like ZnO,[4] SnO_2,[5,6] Nb_2O_5[7] and TiO_2,[8,9] due to their good stability against photocorrosion and excellent electronic properties. Among them, anatase TiO_2, with the highest recorded efficiency 13%, is considered to be one of the best photoanode materials in DSSCs.[10]

In order to obtain higher efficiency, considerable efforts have been made on morphological control of TiO_2 crystals, like nanoparticles, nanorods[11] and nanotubes[12]. The TiO_2 surfaces are in direct contact with the dye molecules and offer anchoring sites for sensitizers. Transmission electron microscopy indicates that anatase TiO_2 powders primarily have {101} faces exposed and {001} facets to a lesser degree.[13] Works on these different crystal facets suggest that the latter {001} facet is more reactive than the former {101} facet and plays a key role in the reactivity of anatase nanoparticles.[14,15] On the other hand, it was only in 2008 that TiO_2 single crystals with high percentage of {001} facets (47%) were fabricated.[16] Since then, TiO_2 crystals with even higher percentage of {001} facets have been reported gradually.[17,18] These achievements provide a new insight for DSSCs fabrication and make it possible for preparing sensitized TiO_2 photoanodes with high percentage of {001} facets ex-

† Corresponding authors
[a] *Key Laboratory of Thermal Management Engineering and Materials, Graduate School at Shenzhen, Tsinghua University, Shenzhen, 518055, China.*
E-mail: lijia@phys.tsinghua.edu.cn. Phone: +86-755-26033022. Fax: +86-755-26036417.
[b] *School of Materials Science and Engineering, Tsinghua University, Beijing, 100084, China.*
[c] *State Key Laboratory of Chemical Resource Engineering, Beijing University of Chemical Technology, Beijing, 100029, China.*
[d] *Department of Physics and State Key Laboratory of Low-Dimensional Quantum Physics, Tsinghua University, Beijing 100084, China.*
[e] *Institute for Advanced Study, Tsinghua University, Beijing, 100084, China.*

posing. In recent years, some experiments show that the DSSCs, with TiO_2 nonocrystal exposing high percentage of {001} faces, have a higher solar light-to-electricity conversion efficiency originated from larger current density, open-circuit voltage and solar absorption.[19–22] However, theoretical investigations on the dye sensitizer adsorption on TiO_2 (001) surface are still scarce and urgently needed to further optimize the photovoltaic performance of DSSCs.

In this work, we have studied the adsorption behavior of dye sensitizer adsorption on (001) surface, comparing with that of dye sensitizer adsorption on (101) surface based on density functional theory (DFT) calculation. N3 molecule, one of the most investigated ruthenium(II) polypyridyl complexes, was used as the sensitizer in our simulation. The N3 molecule is identified as a particularly efficient sensitizer with photo-conversion efficiency higher than 11%.[23] Moreover, it has relatively simple but representative structure, with notable electronic accepter and donor groups and typical carboxylic anchoring groups. We have obtained both energetically preferable structure and adsorbate-induced occupied gap levels in the system of N3 dye adsorption on (001) surface. In addition, adsorption energies as well as energy levels alignment of the N3 molecule adsorption on (001) and (101) surfaces of TiO_2 are also calculated. These results are essential for photovoltaic application and allow us to gain revealing insights into the detailed factors governing the efficiency of DSSCs.

2 Computational details

All calculations were preformed using the Vienna *ab initio* simulation package (VASP) within the framework of DFT.[24–26] The projector augmented plane wave pseudopotentials were employed for the electron-ion interaction.[27] The local density approximation (LDA) exchange-correlation functional was used for structural optimization because it can reproduce the experimental crystal parameters of anatase TiO_2 with an deviation of 0.45% and 0.54% for a and c axes, respectively, compared with the 1.24% and 1.51% by using generalized gradient approximation (GGA). On the other hand, the band gaps of bulk anatase TiO_2 are calculated to be 1.89 eV and 1.87 eV by GGA and LDA methods, respectively, which are consistent with previous result.[28,29] However, due to the self-interaction error,[30] both the LDA and GGA fail to reproduce the experimental band gap of bulk anatase TiO_2 (3.2 eV). Therefore, the electronic properties of N3 molecule, TiO_2 surface and N3 molecule adsorption on TiO_2 surface were calculated using hybrid functional of PBE0, mixing 25% of HF exchange in a PBE scheme.[31] All calculations were performed with a single *k*-point (the Γ point). The cutoff energy for the plane wave basis set was set to 500 eV. The periodically repeated unit cells measured 15.14 Å× 15.14 Å with 9 atomic layers and 16.37 Å× 15.14 Å with 12 atomic layers were adopted for (001) and (101) slabs, respectively. The vacuum distance larger than 15 Å was used in the calculation to remove the interaction between successive TiO_2 slabs. In structural optimization, the lowest three atomic layers were fixed to their bulk truncated positions allowing all others atoms to fully relax until the energy difference between two ionic steps was smaller than 2×10^{-5} eV.

3 Results and discussion

3.1 N3 adsorption on (001) surface.

3.1.1 Adsorption structure and energy.

The optimized structure of TiO_2 (001) surface is depicted in Fig. 1a. In the bulk anatase TiO_2, each Ti atom is octahedrally coordinated to six O atoms, while each O atom is coordinated to three Ti atoms. At TiO_2 surface, both the upmost Ti atoms and bridge O atoms have one coordination vacancy. The fivefold coordinated Ti atoms (Ti_{5c}), 3.78 Å apart in a square lattice, have been proven to be the most favorable anchoring sites for the carboxylic groups of ruthenium polypyridyl complexes.[32,33] In Fig. 1b, the optimized structure of N3 dye molecule shows that Ru atom octahedrally coordinated to six N atoms which are provided by two bipyridyl ligands and two thiocyanate ligands. An approximate C_2 symmetry axis could be found oriented along the bisector of the ∠NRuN angle formed by Ru atom and N atoms of the thiocyanate ligands. In each bipyridyl ligand, two H atoms in para position are substituted by protonated carboxylic groups. Due to the non-coplanarity of these carboxylic groups, it is unlikely that all of them anchor on the TiO_2 surface simultaneously. It is thus that several binding configurations between the N3 dye and the TiO_2 surface should be taken into account, considering the types and numbers of anchoring carboxylic groups. In order to illustrate the anchoring patterns, we have numbered the O atoms of carboxylic groups in Fig. 1b.

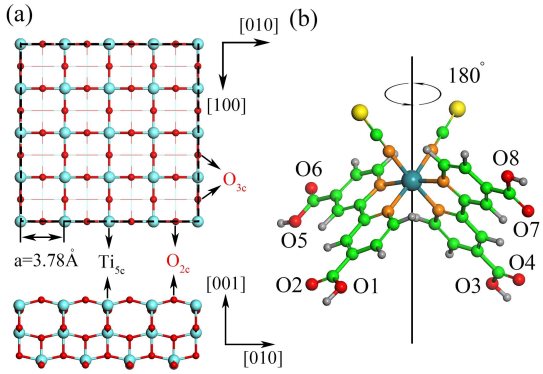

Fig. 1 The optimized structures of (a) TiO_2 (001) surface and (b) N3 dye molecule. Green, red, orange, yellow, gray, aquamarine and cyan spheres represent C, O, N, S, H, Ru and Ti atoms, respectively. The solid line in panel (b) represents the C_2 symmetry axis. Oxygen atoms of dye molecule are numbered in order to clearly depict the adsorption pattern.

Several possible adsorption configurations of the sensitizer on anatase (001) surface are shown in Fig. 2. It is noted that the N3 molecule is put on the surface initially in their fully protonated forms before relaxation. However, irrespective to the bonding types of carboxylic groups with Ti_{5c}, either monodendate or bidentate, the H atoms in carboxylic groups can transfer to the bridge O atoms on TiO_2 surface after relaxation. The similar phenomenon also occurs on the TiO_2 (001) surface with dissociative adsorption of water, methanol,[34] and formic acid.[14] According to our calculation, the valence band maximum (VBM) of TiO_2

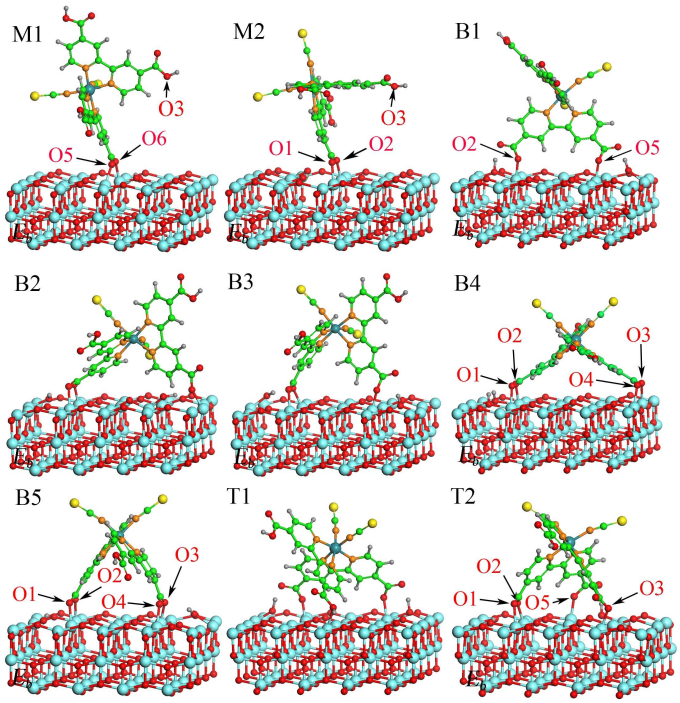

Fig. 2 Different configurations of N3 dyes adsorption on the anatase TiO_2 (001) surface. Configurations B4, B5 and T2 are three most energetically preferable structures. Some oxygen atoms are numbered and referred to in Table 2. Green, red, orange, yellow, gray, aquamarine and cyan spheres represent C, O, N, S, H, Ru and Ti atoms, respectively.

(001) surface is lifted up about 0.64 eV with respect to VBM of TiO_2 (101) surface. The VBM, which is partly contributed by the p orbital of the bridge O_{2c} atom, denotes the high reactivity of surface O atoms and the possibility of capturing H atoms from carboxylic groups. The above result is in agreement with previous findings for formic acid and methanol adsorption on TiO_2 surface.[2,4] The simplest and also the initial attached form of the dye molecule to the anatase surface is a single-bond type (not shown here). Then the rotational motion of the molecule leads to another O atom captured by the Ti_{5c} atom of TiO_2 surface. Because of the approximate C_2 symmetry of N3 molecule, there are only two nonequivalent carboxylic groups which belong to the same bipyridyl ligand. It is shown in Fig. 2 that, for structure M1 (M2), O1 and O2 (O5 and O6) atoms belonging to one carboxylic group form bonds with two Ti_{5c} atoms (Ti_{5c}-O bonds), respectively. In contrast, structure B1 appears with O2 and O5 atoms, belonging to different carboxylic groups, bonding with Ti_{5c} atoms. The average distances between molecular O and surface Ti atoms are about 1.96 Å, 1.96 Å, and 1.94 Å in structures M1, M2 and B1, respectively, indicating stronger bonding for two monodentate coordination than a bidentate bridging coordination.

After the second Ti_{5c}-O bond formation, the rotation of N3 molecules shown in structures M1, M2 and B1 is suppressed partly. There still exist rotation axes passing through the anchoring O atoms, along those the N3 molecules could rotate and more carboxylic groups could attach to the surface. The distance of O5 (O2) and O3 is 9.80 Å (9.95 Å) in isolated N3 molecule, namely 2.59 (2.63) times the distance of two nearest surface Ti_{5c} atoms. Therefore, to form structures B2 and B3 (B4 and B5), different Ti_{5c} atoms along the [010] direction are bonded after rotation of structure M1 (M2). Similarly, if structure B1 tilts along its rotation axis (O2-O5), structure T1 with the third carboxylic group anchoring on TiO_2 (001) surface with nondissociative adsorption (see Fig. S1 of Supporting Information) may appear. Considering the most preferable adsorption configuration of N3 on TiO_2 (101) surface, which has been extensively studied,[33,35] structure T2 shown in Fig. 2 might also be possible.

The adsorption energy (E_b) of N3 molecule is defined by the following expression, $E_b = E_{tot}[slab] + E_{tot}[dye] - E_{tot}[slab + dye]$, where E_{tot} is the total energy of relevant parts.[36] The calculated adsorption energies of N3 molecule in each structure using both LDA and PBE0 methods are shown in Table 1. The adsorption energies obtained by using PBE0 method are about 1∼3 eV less than those calculated by LDA method for each structure. Whereas, structures B4, B5 and T2 are the three most energetically stable structures in both methods.

Table 1 Adsorption energies (eV) of N3 molecules in structures M1∼T2 calculated by LDA and PBE0 methods, respectively.

Structure	M1	M2	B1	B2	B3	B4	B5	T1	T2
LDA	3.69	3.88	3.94	5.10	5.14	6.07	6.12	4.28	6.37
PBE0	2.94	3.03	2.61	3.46	3.81	4.39	4.97	3.04	3.96

Since we concern more about the energetically preferable structures, the Ti_{5c}-O bond lengths of structures B4, B5 and T2 are listed in Table 2. In structures B4 and B5, only bidentate modes of coordination are formed. The lengths of four Ti_{5c}-O bonds in structure B4 are almost identical, while they differ a lot in structure B5. This difference might be due to the influence of H atoms, which attach to the bridge O_{2c} atoms of TiO_2 surface and come from the carboxylic groups. In structure B4, one of the two bridge O_{2c} atoms neighboring to each Ti_{5c}-O bond is attached by H atom, while only the O_{2c} atoms close to O1-Ti and O3-Ti bonds in structure B5 are saturated by H atoms. It is indicated that if an H atom attaches to the nearest surface O_{2c} atom of Ti_{5c}, the length of Ti_{5c}-O bonds will decrease, resulting in the stronger bonding between the surface Ti_{5c} atom and O atom of N3 dye. In structure T2, among the four Ti_{5c}-O bonds, one bidentate and two monodentate modes of coordination are formed. It is clearly seen that, except for O1-Ti bond, each of the other three Ti_{5c}-O bonds is close to a surface O_{2c} atom bonding with H atom, resulting in the decrease in length of Ti_{5c}-O bonds. Moreover, the bond lengths of Ti_{5c}-O bonds in two monodentate modes, especially for O3-Ti, are even shorter than those of Ti_{5c}-O bonds in bidentate mode, consistent with above discussion of stronger bonding for two monodentate coordination than a bidentate bridging coordination.

Table 2 Lengths (in Å) of interfacial Ti_{5c}-O bonds between O atom in N3 molecule and Ti atom on TiO_2 surface. The labeled oxygen atoms referred are shown in Fig. 2

Bond	O1-Ti	O2-Ti	O3-Ti	O4-Ti	O5-Ti
B4	2.04	2.02	2.05	2.01	–
B5	1.99	2.12	1.99	2.03	–
T2	2.04	1.95	1.89	–	1.95

3.1.2 Influence of N3 adsorption patterns on electronic structure.

In DSSCs, the conversion efficiency is mainly determined by the electronic structures of dye molecule and semiconductor. To gain an efficient and stable solar cell, dye molecule should be strongly bound to the underlying semiconductor material and absorb large portion of solar radiation. Deducing from the large adsorption energy, we affirm that N3 molecule forms strong chemisorption bonds with Ti_{5c} on TiO_2 (001) surface. This strong interaction ensures the stability of DSSCs and results in larger amount of molecular adsorption. On the other hand, the light adsorption performance of N3 sensitizer with structure changed is surely influenced. Fig. 3 shows the density of states (DOS) of isolated N3 molecule and the total DOS of N3 molecules with the upmost three atomic layers of TiO_2 slabs of structures B4, B5, T2. It is noted that though N3 molecules are attached to the surface in different modes of coordination, their highest occupied molecular orbitals (HOMO) are all located in the band gap of TiO_2. In addition, the lowest unoccupied molecular orbital (LUMO) of the molecule falls in the conduction band (CB) of the TiO_2 surface for each structure.

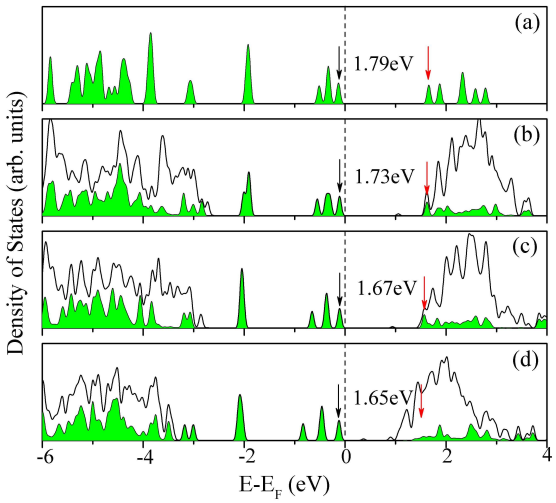

Fig. 3 Density of states (DOS) of (a) isolated N3 molecule, N3 molecules with the upmost three atomic layers of TiO_2 slabs of structures (b) B4, (c) B5 and (d) T2, respectively. Fermi level is represented by the dashed line and set as zero. The contribution of N3 molecule to the DOS is represented by green filled curves.

Due to coupling between electronic states of N3 molecule and the surface, broadening and shifting of both occupied and unoccupied states of the dye around the Fermi level can be clearly observed. The overall effect of shifting results in the narrowing of HOMO-LUMO (pointed out by the black and red arrows in Fig. 3, respectively) gap of N3 molecule and red shifted absorption spectrum of the sensitized TiO_2 surface. Moreover, the effect of gap narrowing increases in sequence of the three structures B4, B5 and T2. While the intensity of LUMO state, which is critical to the light absorption in DSSCs, decreases in the same order. The orbital characteristics of LUMO for different configurations of N3 adsorption on TiO_2 surface are depicted in Fig. 4. For isolated N3 molecule, the LUMO orbital is mainly delocalized on C and N atoms of two bipyridyl ligands,[37] indicating the important role of bipyridyl ligands in electron excitation and transfer. It has been demonstrated that the absorption bands in the visible region are assigned to electrons excited from the Ru-NCS t_{2g}-π^* orbitals to bipyridyl-π^* orbitals.[38] Due to the formation of chemical bonds between surface Ti_{5c} atoms and molecular O atoms, the LUMO of N3 molecule is redistributed, but still delocalized on bipyridyl groups in structures B4 and B5. However, in structure T2, the original LUMO of isolated N3 molecule splits into several orbitals. And the molecular parts of these newly produced orbitals tend to be more localized instead of the original delocalization of π^* orbitals as shown in Fig. 4, thus might induce a negative effect on electron transfer in N3 molecules.

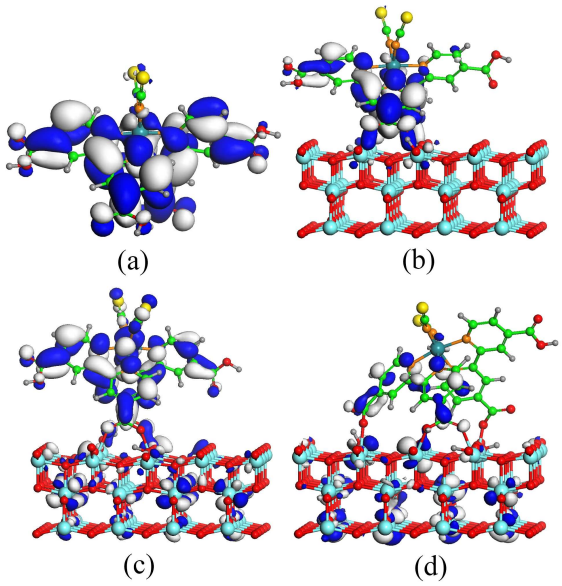

Fig. 4 Isodensity surface plot of (a) lowest unoccupied molecular orbital (LUMO) of isolated N3 molecule and (b-d) crystal orbitals of structure B4, B5 and T2 with the energy levels marked by red arrows in Fig.3. (isodensity values: 0.025 for (a), (b), (c) and 0.015 for (d))

It is intuitive that the N3 dye molecule undergoes larger distortion in structure T2 than in structures B4 and B5. In order to verify the above speculation, the distorted and deprotonated N3 molecules are extracted from structures B4, B5 and T2 for the evaluation of their energy (E_{dis}). Then each N3 molecule is fully relaxed to its ground state to obtain the energy (E_{ref}). The distortion energy is estimated by subtracting E_{ref} from E_{dis}. Comparing the distortion energies of N3 molecules in structure T2, B4 and B5, i.e., 0.43 eV, 0.25 eV and 0.16 eV by LDA method (1.25 eV, 0.51 eV and 0.34 eV by PBE0 method), the N3 molecule in struc-

ture T2 undergoes larger distortion indeed. It seems that structure T2 is easier to be observed in experiments than other structures deducing from the highest adsorption energy calculated by LDA method. However, in actual DSSCs, the TiO_2 nanoparticle and N3 molecule are under a solution condition. In consideration of the adsorption of solvent molecules, structure B5 could be more preferable than structure T2 (discussion in the Supporting Information). Moreover, it is obvious that the larger distortion of N3 molecule in structure T2 will increase the difficulty of the formation of structure T2. Combining the adsorption energy calculated by PBE0 hybrid functional and the influence of solvent molecule, it is suggested that structure B5 might be the dominant structure in N3/TiO_2 complex if (001) surfaces are exposed in DSSCs. So if not explicitly mentioned, structure B5 will be used for discussion in the following sections.

3.2 N3 adsorption on TiO_2 (101) surface.

To make a comparison between N3 adsorption on different surfaces of TiO_2, the adsorption behavior of N3 on TiO_2 (101) surface is also investigated shown in Fig. S3 of Supporting Information). The (101) surface is the thermodynamically stable surface in TiO_2 nanocrystal, and has been extensively investigated in theory before.[14,39–41] Unlike (001) surface, O_{2c} atoms in (101) surface tend to be more inert. It is found that the H atoms of carboxylic groups do not spontaneously transfer to the O_{2c} atom of (101) surface after relaxation. Similar results have been observed in other adsorbate like H_2O, methanol,[42] and formic acid.[43] However, experimental results show that the adsorbed N3 molecules contains both -CO_2^- groups and C=O bonds,[32] indicating part of carboxylic acid groups should be deprotonated. This discrepancy is ascribed to the solution condition in experiments and zero temperature assumption in theoretical calculations. To mimic the experimental results, two H atoms from N3 sensitizer are initially transferred to their nearest O_{2c} atoms for structural relaxation. Among several possible configurations, the most preferable one noted as E1 is shown in Fig. 5. In this structure, N3 anchors on (101) surface dissociatively with a bidentate and two monodentate modes of coordination, indicating that the dye molecule is more likely to be adsorbed on (101) surface in the form of partly deprotonated.[33,35]

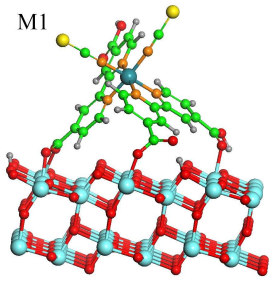

Fig. 5 The most preferable configurations of N3 adsorption on TiO_2 (101) surface. Green, red, orange, yellow, gray, aquamarine and cyan spheres represent C, O, N, S, H, Ru, and Ti atoms, respectively.

3.3 Comparison of N3 adsorption on (001) and (101) surfaces.

The bonding of N3 with TiO_2 (101) surface, with adsorption energies of 3.84 eV calculated by LDA method and 1.55 eV calculated by PBE0 method, is considerably weaker than that of N3 with TiO_2 (001) surface. In order to explain the difference of adsorption energy, projected density of states (PDOS) of Ti_{5c} atoms on (001) and (101) surfaces are shown in Fig. 6. It is noted that there are extra states in the energy range of -8.0 eV $\sim$ -7.0 eV for clean (001) surface, compared with those of (101) surface. After the adsorption of N3 molecule, the intensity of states provided by Ti_{5c} in this energy range decreases sharply, due to the chemical bonding with carboxylic groups in N3 molecule. The insert in Fig. 6a shows the contribution of 3*d* orbitals of Ti_{5c} on clean (001) surface in this energy range. It is suggested a strong coupling of 3*d* orbitals of Ti_{5c} (mainly from d_{xy} and d_{yz} orbitals) with 2*p* orbitals of O atoms in N3 molecule, resulting in the downshift of 3*d* orbitals of Ti_{5c} atoms to deeper energy level. However, for (101) surface, the occupied states of Ti_{5c} atoms are mainly located inside the deeper energy range and contribute a little to the VBM of the (101) surface. It is thus that the shift in energy of 3*d* states of Ti_{5c} atoms after bonding with N3 molecule is relatively smaller. Moreover, the almost unchanged PDOS of Ti_{5c} near the Fermi level of (101) surface indicates that the interaction of Ti_{5c} with N3 is relatively weaker than that of (001) surface. Consequently, the adsorption energy of N3 on (001) surface is much larger than that of N3 on (101) surface.

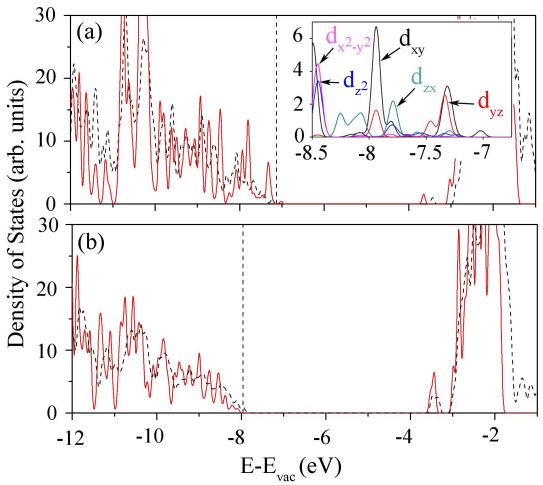

Fig. 6 Projected density of states (PDOS) of surface Ti atoms on (a) (001) and (b) (101) surfaces. Red solid and black dashed lines represent PDOS of Ti atoms in clean and adsorbed surface, respectively. Dashed vertical lines correspond to Fermi levels of clean surface. The insert in panel (a) shows DOS projected on the 3*d* orbitals of Ti_{5c} atoms on clean (001) surface.

Total DOS and PDOS of N3 molecules adsorption on (001) and (101) surfaces are shown in Fig. 7 to make a comparison of DSSC-related performance between two systems. In order to align their energy levels, vacuum energy is set to zero in both two systems. Despite the difference of broadening in conduction and valence band of the oxide, the states of N3, located in the band gap of

oxides, differ by little between two systems. It is indicated that the electron donor groups are not strongly influenced by the TiO_2 surface. In addition, the LUMO-HOMO gap, 1.67 eV for both systems, shows that the absorption spectrum does not change much even when more {001} faces are exposed in TiO_2 nanoparticles. However, for N3 adsorption on (001) surface, the shift-down of both occupied and unoccupied states of the dye around the Fermi level results in a decrease of energy difference between LUMO of N3 and conduction band minimum (CBM) of TiO_2, changing from 0.9 eV for (101) surface to 0.6 eV for (001) surface. In addition, although the CBMs in both systems are provided by *d* orbitals of Ti atoms (shown in Fig. S4 of Supporting Information), the level position of CBM of N3 adsorption on (001) surface is slightly higher (about 60 meV) than that of N3 on (101) surface, suggesting a higher power potential in DSSCs where photoanode materials are made by TiO_2 nanoparticles exposing more {001} faces.

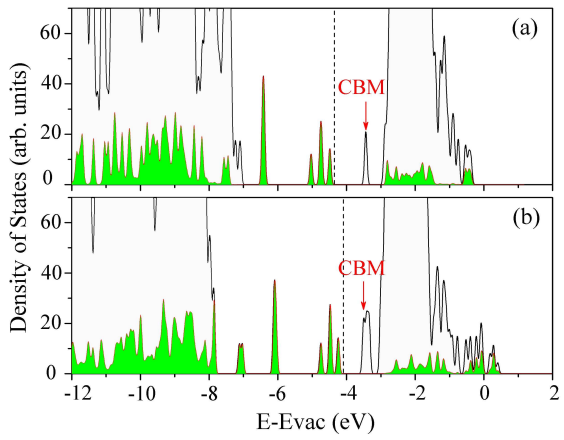

Fig. 7 DOS of N3 adsorption on TiO_2 (a) (001) and (b) (101) surfaces. The contribution of N3 molecule to the DOS is represented by green filled curves. Dash vertical lines correspond to Fermi levels. Vacuum levels are used in energy levels alignment.

4 Conclusion

In summary, we have systematically investigated the adsorption behavior of N3 sensitizers on (001) surfaces of anatase TiO_2. Our results show that structure B5, where N3 molecule anchors with its two carboxyl groups coordinated via bidentate coordination to the Ti_{5c} atoms of TiO_2 surface, is believed to be the most easily formed structure. The adsorption energy of N3 molecule on TiO_2 (001) surface is large enough to enable the formation of dense dye molecular layers on anatase nanoparticles, not only resulting in a higher absorptivity of solar radiation, but also lowering the dark current produced by interaction between TiO_2 and mediator in solution. Our study also reveals that the LUMO-HOMO gap of N3 molecule decreases about 0.12 eV upon adsorption, suggesting an ever larger range of absorption spectrum than isolated N3 molecule. In addition, the LUMO of N3 is still delocalized on bipyridyl groups and overlapped with some orbitals of TiO_2, providing paths for easy electron transfer from N3 molecule to TiO_2. And the higher CBM of TiO_2 (001) surface with N3 adsorption, compared with that of (101) surface, indicates the higher open circuit potential. These results can provide practical guidance to the development of TiO_2 particles with exposing more {001} faces as promising photoanode materials in DSSCs.

Acknowledgements

This work was supported by the Ministry of Science and Technology of China (Grant No. 2011CB606405), the National Nature Science Foundation of China (Grant No. 11104155, 51232005, and 51202121), Shenzhen Projects for Basic Research (Grant Nos. JC201105201119A, JCYJ20120831165730910, and KQCX20140521161756227), Guangdong Province Innovation R & D Team Plan for Energy and Environmental Materials (Grant No. 2009010025). Computational resources from the TIANHE-1 in the Tianjin Supercomputing Center are also acknowledged.

References

1 M. Grätzel, *Nature*, 2001, **414**, 338–344.
2 N. Robertson, *Angew. Chem. Int. Ed.*, 2006, **45**, 2338–2345.
3 J. T. Wallmark, *Proc. IRE*, 1957, **45**, 474–483.
4 M. Saito and S. Fujihara, *Energy Environ. Sci.*, 2008, **1**, 280–283.
5 A. Kay and M. Grätzel, *Chem. Mater.*, 2002, **14**, 2930–2935.
6 H. J. Snaith and C. Ducati, *Nano Lett.*, 2010, **10**, 1259–1265.
7 K. Sayama, H. Sugihara and H. Arakawa, *Chem. Mater.*, 1998, **10**, 3825–3832.
8 B. O'regan and M. Grätzel, *Nature*, 1991, **353**, 737–740.
9 C. S. Kley, C. Dette, G. Rinke, C. E. Patrick, J. Čechal, S. J. Jung, M. Baur, M. Dürr, S. Rauschenbach, F. Giustino *et al.*, *Nano Lett.*, 2014, **14**, 563–569.
10 S. Mathew, A. Yella, P. Gao, R. Humphry-Baker, B. F. E. Curchod, N. Ashari-Astani, I. Tavernelli, U. Rothlisberger, M. K. Nazeeruddin and M. Grätzel, *Nat. Chem.*, 2014, **6**, 242–247.
11 P. D. Cozzoli, A. Kornowski and H. Weller, *J. Am. Chem. Soc.*, 2003, **125**, 14539–14548.
12 G. K. Mor, K. Shankar, M. Paulose, O. K. Varghese and C. A. Grimes, *Nano Lett.*, 2006, **6**, 215–218.
13 A. Zaban, S. Aruna, S. Tirosh, B. Gregg and Y. Mastai, *J. Phys. Chem. B*, 2000, **104**, 4130–4133.
14 X.-Q. Gong, A. Selloni and A. Vittadini, *J. Phys. Chem. B*, 2006, **110**, 2804–2811.
15 A. Vittadini, A. Selloni, F. Rotzinger and M. Grätzel, *Phys. Rev. Lett.*, 1998, **81**, 2954.
16 H. G. Yang, C. H. Sun, S. Z. Qiao, J. Zou, G. Liu, S. C. Smith, H. M. Cheng and G. Q. Lu, *Nature*, 2008, **453**, 638–641.
17 X. Han, Q. Kuang, M. Jin, Z. Xie and L. Zheng, *J. Am. Chem. Soc.*, 2009, **131**, 3152–3153.
18 H. G. Yang, G. Liu, S. Z. Qiao, C. H. Sun, Y. G. Jin, S. C. Smith, J. Zou, H. M. Cheng and G. Q. Lu, *J. Am. Chem. Soc.*, 2009, **131**, 4078–4083.
19 W. Q. Fang, X. H. Yang, H. Zhu, Z. Li, H. Zhao, X. Yao and H. G. Yang, *J. Mater. Chem.*, 2012, **22**, 22082–22089.
20 J. Yu, J. Fan and K. Lv, *Nanoscale*, 2010, **2**, 2144–2149.
21 H. Zhang, Y. Han, X. Liu, P. Liu, H. Yu, S. Zhang, X. Yao and H. Zhao, *Chem. Commun.*, 2010, **46**, 8395–8397.

22 X. Wu, Z. Chen, G. Q. M. Lu and L. Wang, *Adv. Funct. Mater.*, 2011, **21**, 4167–4172.

23 C.-Y. Chen, M. Wang, J.-Y. Li, N. Pootrakulchote, L. Alibabaei, C.-h. Ngoc-le, J.-D. Decoppet, J.-H. Tsai, C. Grätzel, C.-G. Wu *et al.*, *ACS nano*, 2009, **3**, 3103–3109.

24 G. Kresse and J. Hafner, *Phys. Rev. B*, 1993, **48**, 13115.

25 G. Kresse and J. Furthmüller, *Phys. Rev. B*, 1996, **54**, 11169.

26 G. Kresse and J. Furthmüller, *Comp. Mater. Sci.*, 1996, **6**, 15–50.

27 G. Kresse and D. Joubert, *Phys. Rev. B*, 1999, **59**, 1758.

28 M. Landmann, E. Rauls and W. Schmidt, *J. Phys.: Condens. Matter*, 2012, **24**, 195503.

29 F. Labat, P. Baranek, C. Domain, C. Minot and C. Adamo, *J. Chem. Phys.*, 2007, **126**, 154703.

30 J. P. Perdew and M. Levy, *Phys. Rev. Lett.*, 1983, **51**, 1884–1887.

31 C. Adamo and V. Barone, *J. Chem. Phys.*, 1999, **110**, 6158–6170.

32 K. S. Finnie, J. R. Bartlett and J. L. Woolfrey, *Langmuir*, 1998, **14**, 2744–2749.

33 F. Schiffmann, J. VandeVondele, J. Hutter, R. Wirz, A. Urakawa and A. Baiker, *J. Phys. Chem. C*, 2010, **114**, 8398–8404.

34 P. Persson and M. J. Lundqvist, *J. Phys. Chem. B*, 2005, **109**, 11918–11924.

35 F. De Angelis, S. Fantacci, A. Selloni, M. K. Nazeeruddin and M. Grätzel, *J. Phys. Chem. C*, 2010, **114**, 6054–6061.

36 D. Çakır, O. Gülseren, E. Mete and Ş. Ellialtıoğlu, *Phys. Rev. B*, 2009, **80**, 035431.

37 M. K. Nazeeruddin, F. De Angelis, S. Fantacci, A. Selloni, G. Viscardi, P. Liska, S. Ito, B. Takeru and M. Grätzel, *J. Am. Chem. Soc.*, 2005, **127**, 16835–16847.

38 S. Fantacci, F. De Angelis and A. Selloni, *J. Am. Chem. Soc.*, 2003, **125**, 4381–4387.

39 W. Hebenstreit, N. Ruzycki, G. S. Herman, Y. Gao and U. Diebold, *Phys. Rev. B*, 2000, **62**, R16334.

40 P. Scheiber, M. Fidler, O. Dulub, M. Schmid, U. Diebold, W. Hou, U. Aschauer and A. Selloni, *Phys. Rev. Lett.*, 2012, **109**, 136103.

41 J. Pan, G. Liu, G. Q. M. Lu and H.-M. Cheng, *Angew. Chem. Int. Ed.*, 2011, **50**, 2133–2137.

42 G. S. Herman, Z. Dohnalek, N. Ruzycki and U. Diebold, *J. Phys. Chem. B*, 2003, **107**, 2788–2795.

43 A. Vittadini, A. Selloni, F. Rotzinger and M. Grätzel, *J. Phys. Chem. B*, 2000, **104**, 1300–1306.